
Dynamic Differential-Privacy Preserving SGD

Jian Du^{*1} Song Li^{*2} Xiangyi Chen^{*3} Siheng Chen² Mingyi Hong³

Abstract

The vanilla Differentially-Private Stochastic Gradient Descent (DP-SGD), including DP-Adam and other variants, ensures the privacy of training data by uniformly distributing privacy costs across training steps. The equivalent privacy costs controlled by maintaining the same gradient clipping thresholds and noise powers in each step result in unstable updates and a lower model accuracy when compared to the non-DP counterpart. In this paper, we propose the dynamic DP-SGD (along with dynamic DP-Adam, and others) to reduce the performance loss gap while maintaining privacy by dynamically adjusting clipping thresholds and noise powers while adhering to a total privacy budget constraint. Extensive experiments on a variety of deep learning tasks, including image classification, natural language processing, and federated learning, demonstrate that the proposed dynamic DP-SGD algorithm stabilizes updates and, as a result, significantly improves model accuracy in the strong privacy protection region when compared to the vanilla DP-SGD. We also conduct theoretical analysis to better understand the privacy-utility trade-off with dynamic DP-SGD, as well as to learn why Dynamic DP-SGD can outperform vanilla DP-SGD.

1. Introduction

Publishing deep neural networks trained on private datasets poses a significant risk of data privacy leakage because the model embeds information about the training data. [Zhu & Han \(2020\)](#) and [Zhao et al. \(2020\)](#), for example, both provide paradigms for breaching privacy and reconstructing training examples from published models. As a result, optimizers that protect the privacy of the model while training it are becoming increasingly important. Differential

Privacy (DP) ([Dwork, 2006](#)), a gold-standard method for privacy-preserving computation that makes it nearly impossible for an adversary to single out a data record, is growing in importance and must be guaranteed to protect privacy.

By clipping the per-sample gradient and adding calibrated Gaussian noise in each step, Differentially-Private SGD (DP-SGD) ([Abadi et al., 2016](#)) has been proposed to protect the model with the corresponding total privacy cost derived by composing the privacy costs of each step being less than a predefined privacy budget. The clipping operation, which causes estimation bias to the true gradient, as well as the random noise, induce instability and even ramp-up of DP-SGD updates, as illustrated by the test shown in [Fig. 1](#). A high clipping threshold, intuitively, implies a small bias term, and vice versa. Under a fixed privacy, thereby, we can reduce bias by using large clipping thresholds, but at the costs of possible performance degradation due to increased noise power.

In the vanilla DP-SGD, a constant clipping threshold is used, and choosing the proper clipping threshold, according to the literature, is more of an art than a science. This motivates us to study how to adapt to the dynamic of private gradient updates to adjust the clipping threshold and noise power so as to narrow the performance gap from both the practical implementation as well as theoretical understanding point of views. In this paper, we make the following main contributions:

- We extend the Gaussian DP’s central limit theorem (CLT) to obtain an analytical composition results for non-uniform distributing privacy costs with the Gaussian mechanisms. The closed-form expression of the CLT result facilitates the dynamic clipping and noise calibration along the updates under a predefined privacy budget constraint. We thereby propose the *sensitivity decay* and *growing- μ_t* methods under this extended Gaussian DP CLT, and show that combining these two methods leads to a novel *dynamic DP-SGD* algorithm with additional performance gain in practice.
- We perform a series of experiments and ablation studies on a variety of neural network tasks, including image classification, natural language processing, and federated learning, and show that the proposed dy-

^{*}Equal contribution ¹Ant Group, Sunnyvale, CA ²Shanghai Jiao Tong University, China ³University of Minnesota, MN. Correspondence to: Jian Du <jd.jiandu@gmail.com>.

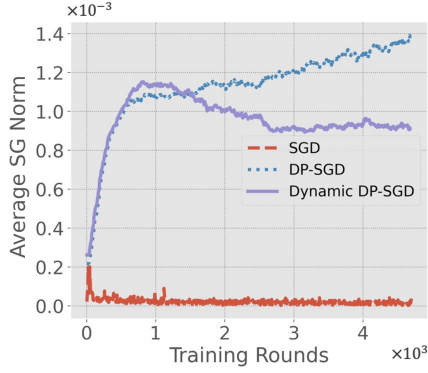


Figure 1. Experiments on MNIST with DP budget $(\epsilon, \delta) = (0.4, 10^{-5})$ after 5×10^3 steps for both DP-SGD and the proposed dynamic DP-SGD with the same corresponding settings as that in Table 1. In comparison to SGD, DP-SGD is unstable, and the stochastic gradient (SG) norm has a ramp-up period. However, the SG norm is stabilized by the dynamic DP-SGD. Additional experiments on the Fashion-MNIST is also provided in Appendix A.1.

dynamic DP-SGD effectively stabilizes gradient updates and consistently outperforms existing methods. With a strong privacy guarantee, i.e., at $\epsilon = 1.2$, dynamic DP-SGD has a performance loss of only 2.49% when compared to the non-DP version on MNIST dataset, and the loss is reduced to 1.72% in the federated learning setting for a stronger privacy guarantee, i.e., $\epsilon = 1$.

- We investigate analytically the impact of varying DP costs along the updates, and derive the utility guarantee of the proposed DP-SGD method. Mathematically, we demonstrate the utility on both clipping thresholds and noise powers over iterations, and we gain insights into the privacy-utility trade-off with dynamic DP-SGD.

2. Differential Privacy and Vanilla DP-SGD

Differential Privacy (DP) defines an upper bound of the privacy level by computing a pair of $(\epsilon, \delta(\epsilon))$. A lower ϵ value leads to better privacy protection, but it potentially also makes the protected algorithm less useful. The value δ can be interpreted as the probability of failing to achieve DP. With the notion of the neighboring data sets, i.e., $X \sim X'$, which differs by one *data record*, the formal (ϵ, δ) -DP definition is given below (Dwork, 2006).

Definition 1. ($(\epsilon, \delta(\epsilon))$ -DP Profile) A randomized algorithm $M(\cdot)$ gives $(\epsilon, \delta(\epsilon))$ -differential privacy if for any pair of neighboring datasets $X \sim X'$ and any event E belongs to the range of M ,

$$\mathbb{P}(M(X) \in E) \leq e^\epsilon \mathbb{P}(M(X') \in E) + \delta,$$

where the probability $\mathbb{P}(\cdot)$ is taken over the randomness

of M , and $\epsilon \geq 0$. When $\delta = 0$, the algorithm is ϵ -DP. Intuitively, this means that we can't tell whether M was run on X or X' based on the results. Thereby, an adversary will almost never infer the existence of any specific data record in the input data set.

In a Gaussian DP mechanism, let Y be the random variable following Gaussian distribution with $Y \sim \mathcal{N}(0, \sigma^2 I_d)$ and $f: X^n \rightarrow \mathbb{R}^d$. The Gaussian mechanism $M(X) = f(X) + Y$ follows the DP profile (Wang et al., 2019):

$$\delta(\epsilon; \mu) = \Phi\left(-\frac{\epsilon}{\mu} + \frac{\mu}{2}\right) - e^\epsilon \Phi\left(-\frac{\epsilon}{\mu} - \frac{\mu}{2}\right), \quad (1)$$

where

$$\mu = \frac{C}{\sigma}, \quad (2)$$

with C the sensitivity of $f(X)$ and $\Phi(\cdot)$ the Gaussian cumulative distribution function. The DP-SGD, which protects the model from revealing the training data privacy, is proposed in Abadi et al. (2016) based on the Gaussian mechanism. Let the model parameters be denoted by θ . and the loss function be $L(\theta) = \frac{1}{N} \sum_{i=1}^N f(\theta, x_i)$ and the clipped stochastic gradient at step t as $g_t = \frac{1}{p|X|} [\sum_{x \in X_t} \text{CL}(g_x; C_t)]$ where $g_x \triangleq \frac{\partial f(\theta_t, x)}{\partial \theta_t}$. To calibrate the noise required for DP, one can first clip the ℓ_2 -norm of the gradient by computing

$$\tilde{g}_x \triangleq \text{CL}(g_x; C) \triangleq g_x \cdot \min\left(1, \frac{C}{\|g_x\|}\right), \quad (3)$$

and then add the noise $\xi_t \sim \mathcal{N}(0, \sigma^2)$ with $\sigma^2 = \frac{C^2}{\mu^2}$. That is, the t -th step of the DP-SGD algorithm is given by:

$$\text{DP-SGD: } \theta_{t+1} = \theta_t - \eta \frac{1}{|X_t|} \left(\sum_{x \in X_t} \tilde{g}_x + \xi_t \right). \quad (4)$$

Because of DP's post-processing property (Dwork et al., 2014, Proposition 2.1), protecting gradients provides the same level of privacy protection on the output model. A closer examination of the DP-SGD process in (4) reveals that the clipping-per-sample operator introduces biases to the original unbiased gradient estimate in the SGD updates if C is not large enough. It is possible to have an unbiased gradient estimate by increasing C , if C is greater than any ℓ_2 norm of $\frac{\partial f_x}{\partial \theta}$. It does, however, result in an over-calibrated noise power.

Motivations of this work: In standard SGD updates for non-convex optimization, it has been shown that $\lim_{T \rightarrow \infty} \mathbb{E} \left[\|\partial f(\theta_T, x) / \partial \theta_T\|^2 \right] = 0$ (Bottou et al., 2018). However, because the vanilla DP-SGD is followed by fixed clipping threshold C and constant noise power σ^2 as shown in Eq.(3) and (4), the ratio of noise power to the true gradient norm in Eq. (4) would continue to rise if

$\lim_{T \rightarrow \infty} \mathbb{E} \left[\|\partial f(\theta_T, x) / \partial \theta_T\|^2 \right] = 0$, resulting in unstable updates. This hypothesis is supported by the experimental results in Fig. 1 as well as that displayed in Appendix A.1, which display the average coordinate stochastic gradient norm for all the data records in each step. It is worth noting that the stochastic gradient norm has a ramp-up period. Similar phenomenon also appeared in the experiments in (Thakkar et al., 2019, Fig. 4). The observation motivates us to investigate a dynamic DP-SGD to change C and σ^2 along with the stochastic gradient updates in order to stabilize the iterations. To facilitate the study, in the following section, we extend the Gaussian DP CLT (Dong et al., 2019) to compose the non-uniformly DP costs.

3. Dynamic DP-SGD

In the following, we evaluate the privacy cost using the Gaussian DP (GDP) framework (Dong et al., 2019), which measures the privacy profile (ϵ, δ) in terms of $\mu = C/\sigma$ using Eq. (1) and (2). To make our paper self-contained, we include a preliminary of GDP in Appendix A.2.

3.1. Extended CLT for GDP

Existing GDP CLT results (Dong et al., 2019; Bu et al., 2020) assume that each step satisfies the same G_μ -DP, which is insufficient for the dynamic changing C and σ case. We investigate the extended GDP CLT to pave the way for privacy accounting of dynamic DP-SGD, in which each step t has different C_t and σ_t , resulting in different G_{μ_t} -DP costs to be composed. Let M_A and M_B denote the compositions of T steps updates of the training data sets X and X' , respectively, with $X \sim X'$. According to (4), each step consists of sub-sampling, denoted by $\text{PS}(\cdot)$ and local updates. Then, we express M_A and M_B by the composition of T -step updates, respectively,

$$M_A \triangleq M_T \circ \text{PS}_T(X) \circ \dots \circ M_1 \circ \text{PS}_1(X)$$

$$M_B \triangleq M_T \circ \text{PS}_T(X') \circ \dots \circ M_1 \circ \text{PS}_1(X').$$

Consider the sampling scheme $\text{PS}(X)$ that each individual data sample (x, y) is subsampled independently with probability p from the training set to construct X_t . It is shown (Bu et al., 2020) that a particular trade-off function T as defined in Appendix A.2 satisfies:

$$\text{T}(M_A, M_B) \geq \otimes_{t=1}^T (p \cdot G_{\mu_t} + (1-p) \text{Id}), \quad (5)$$

where G_{μ_t} is a function of $\mathcal{N}(0, 1)$ and $\mathcal{N}(\mu_t, 1)$ with $\mu_t = C_t/\sigma_t$ and $\text{Id}(\alpha) = 1 - \alpha$. The details of functions T and $G_\mu(\alpha)$ are given in the appendix. The symbol $\otimes_{t=1}^T$ denotes the product of all the T trade-off functions with the form $p \cdot G_{\mu_t} + (1-p) \text{Id}$, which is far from analytically computable. When all μ_t are the same, i.e., $\mu_t = \mu$, Bu et al.

(2020) shows the CLT of the composition is given by

$$\mu_{\text{tot}} = p \sqrt{T(e^{\mu^2} - 1)}. \quad (6)$$

In the following corollary, we develop an extension of the above GDP CLT with the proof provided in Appendix A.

Corollary 1. *Consider a series of adaptive composition mechanisms M_t for $t \in [T]$, where M_t is G_{μ_t} -DP, and each mechanism works only on a subsampled data sets by independent Bernoulli trial with probability p . The trade-off function for $\lim_{T \rightarrow \infty} \otimes_{t=1}^T (p \cdot G_{\mu_t} + (1-p) \text{Id})$ in (5) approaches to $G_{\mu_{\text{tot}}}$ -DP when $p\sqrt{T}$ is a constant, where*

$$\mu_{\text{tot}} = p \cdot \sqrt{\sum_{t=1}^T (e^{\mu_t^2} - 1)}, \quad (7)$$

and $\mu_t = C_t/\sigma_t$. Notably, when $\mu_t = \mu$ is substituted for $t \in [T]$, Eq. (7) reduces to the CLT result in (6). Similar to the original GDP CLT (Dong et al., 2019; Bu et al., 2020), μ_{tot} is an approximation of the privacy cost after T steps by CLT-type composition of Gaussian mechanism. We demonstrate numerically in Fig. 4 later in the experimental results section that only after hundreds of steps (much less than an epoch), this approximate result approaches its upper bound computed by advanced RDP (Balle et al., 2020). For more details about RDP and the convergence verification of the GDP CLT, please refer to the explanation for Fig. 4.

Corollary 1 reflects that, given the target privacy budget (ϵ, δ) and the corresponding privacy parameter μ_{tot} obtained by (1), we can proactively allocate privacy cost to each step $t \in [T]$ for a predefined total number of steps T , according to (7). We can adjust both C_t and σ_t to control the privacy budget allocation. Section 3.2-Section 3.4 detail the corresponding algorithms.

3.2. Growing- μ_t Method

According to the discussion at the end of Section 2, it is expected that the stochastic gradient norm decreases in expectation along the updates. However, vanilla DP-SGD with constant σ leads to an increasing noise power to true gradient ratio with proper C , under which the stochastic gradient would not be clipped after some t if its norm becomes smaller than C in the ideal case. If so, it is natural to reduce the noise power to stabilize the gradient updates. Thereby, we investigate a method to reduce the noise power σ_t while keeping $C_t = C$. According to Eq. (2), $\mu_{t+1} \geq \mu_t$ for all $t \in [T]$ in this case, and we therefore term this method as Growing- μ_t . With (7) in mind, we control the privacy cost rate by adjusting a hyper-parameter ρ_μ with

$$\rho_\mu \triangleq \frac{\mu_T}{\mu_0}, \quad \rho_\mu \geq 1. \quad (8)$$

Algorithm 1 μ_t computation

Require: privacy budget (ϵ, δ) , T , ρ_μ .

- 1: Compute μ_{tot} corresponding to (ϵ, δ) according to (1).
- 2: Compute μ_0 in (10) by binary search.
- 3: Compute σ_t according to (11) for all $t \in [T]$.

Then the dynamic μ_t is given by

$$\mu_t = (\rho_\mu)^{t/T} \cdot \mu_0, \quad \forall t \in [T]. \quad (9)$$

Given the total privacy budget (ϵ, δ) , the equivalent privacy parameter μ_{tot} is obtained according to (1). Then the remaining problem is to determine the initial state μ_0 . Once μ_0 is obtained, the entire $\{\mu_t\}$ sequence can be generated according to (9). By substituting (9) into (7), we obtain

$$\mu_{\text{tot}}^2 = p^2 \cdot \sum_{t=1}^T \left(\exp \left\{ \left((\rho_\mu)^{t/T} \cdot \mu_0 \right)^2 \right\} - 1 \right). \quad (10)$$

Because the above equation is transcendental when $\rho_\mu > 1$, there is no closed-form solution for μ_0 . Nonetheless, the r.h.s of (10) is monotone increasing w.r.t. μ_0 , and we can thus solve it efficiently using a numerical method such as binary search. The computation of μ_t is summarized in Algorithm 1¹. The noise power at iteration t can be calculated using a specific expression of μ_0 and ρ_μ :

$$\sigma_t = \frac{C}{\mu_0} (\rho_\mu)^{-\frac{t}{T}}, \quad \rho_\mu > 1, \quad \forall t \in [T]. \quad (11)$$

One numerical example is shown in Fig. 2. Given the total DP budget $\epsilon = 1.2$, growing- μ_t gives the freedom to adjust the privacy cost rate, which is the slope of the curve. In Fig 2, we demonstrate the privacy budget consumption curve for different ρ_μ . The solid line ($\rho_\mu = 1$) represents vanilla DP-SGD with evenly distributed noise power along with the step updates. With growing- μ_t , we can now realize any μ consumption process under the constraint of the total DP budget as shown by the dashed lines. Specifically, the growing- μ_t slows consumption in the early rounds and accelerates consumption in the later rounds.

3.3. Sensitivity-Decay Method

When the required level of privacy protection is high, i.e., a small μ_{tot} , it requires a large $1/\mu_t = \sigma_t/C_t$ according to Eq. (7). If C_t is larger than the (stochastic) gradient norm, the noise, which is calibrated by C_t , will dominate the true gradient and could lead to unstable DP-SGD updates as

¹The privacy cost rate form in (8) is not the only one; Trying different forms requires more heuristic work, and it also makes the theoretical analysis of privacy-utility trade-off later more involved.

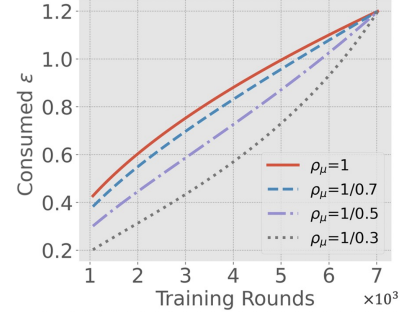


Figure 2. Consumption of privacy budget with different μ_t increasing rates; $\epsilon = 1.2$.

shown in Fig. 1. Based on this observation and considering the previous discussion that the stochastic gradient norm should be decreased in expectation to ensure the convergence, we design to reduce C_t across the updates. Compare to the constant C case in vanilla DP-SGD, it will reduce the required noise power after a particular t when $C_t < C$.

Towards this end, we set the sequence of clipping values as follows

$$C_t = (\rho_c)^{-\frac{t}{T}} \cdot C_0, \quad \rho_c \geq 1, \quad \forall t \in [T]. \quad (12)$$

Different from the growing- μ_t method, we fix $\mu_t = \mu_0$. By further substituting $\mu_t = \mu_0$ into (7) in Theorem 1, we have the closed-form solution:

$$\mu_0 = \sqrt{\log \left(\frac{\mu_{\text{tot}}^2}{p^2 T} + 1 \right)}, \quad t \in [T]. \quad (13)$$

With (12) and (13), we can calibrate the noise power at each step by:

$$\sigma_t = \frac{C_0}{\mu_0} (\rho_c)^{-\frac{t}{T}}, \quad \rho_c > 1, \quad t \in [T]. \quad (14)$$

3.4. Dynamic DP-SGD

Algorithm 2 Dynamic DP-SGD Algorithm

Require: DP budget (ϵ, δ) , sampling rate p and hyper-parameters: ρ_μ , ρ_c and C_0 .

- 1: Compute μ_0 in Algorithm 1
- 2: **for** $t = 1, \dots, T$ **do**
- 3: Compute $C_t = (\rho_c)^{-\frac{t}{T}} \cdot C_0$ in (12)
- 4: Calibrate noise : $\sigma_t = \frac{C_0}{\mu_0} (\rho_\mu \cdot \rho_c)^{-\frac{t}{T}}$
- 5: Sample $X_t \in X$ with sampling rate p and sample noise $\xi_t \sim \mathcal{N}(0, \sigma_t^2 I)$.
- 6: Compute: $\theta_{t+1} = \theta_t - \frac{\eta}{|X_t|} [\xi_t + \sum_{x \in X_t} \text{CL}(g_x; C_t)]$ with $\text{CL}(\cdot)$ given in (3)
- 7: **end for**

Because the noise calibration is based on C_t , we incorporate the growing- μ_t method into the sensitivity-decay method and refer to this new one as dynamic DP-SGD. It maintains the same μ_t increasing rate as the previous growing- μ_t method while having a faster noise decay rate than the sensitivity-decay method. We summarize the dynamic DP-SGD algorithm in Algorithm 2 and conduct extensive experiments to show how dynamic DP-SGD improves performance.

Remark on the dynamic private version of other optimizers: DP version of other optimizers besides SGD can benefit from the proposed dynamically changing clipping thresholds and noise powers. A private version of Adam, which is refer to as dynamic DP-Adam, for example, can be obtained similar by first computing the average per-sample gradient using Line 6 in Algorithm 2, i.e., $\frac{1}{|X_t|} [\xi_t + \sum_{x \in X_t} \text{CL}(g_x; C_t)]$. According to the post-processing property of DP (Dwork et al., 2014, Proposition 2.1), the first and second moments of the gradient can be computed based on this DP guaranteed result, and accordingly the DP version of Adam can be computed with details provided in Appendix A.4. Similarly, we can derive DP version of AdaGrad, RMSProp, etc.

4. Experiments

4.1. Datasets, Models and Benchmarks

Datasets: To conduct a comprehensive test of the dynamic DP-SGD performance, we run experiments with neural network models including MLP, CNN, LSTM, Federated Learning, and VGG-11 on the following 6 datasets: MNIST, FashionMNIST, IMDB, NAME, InfiniteMNIST, and chest radiographs from the Paediatric Pneumonia dataset (Keremany et al., 2018). In Appendix A.9, we describe each data set, the corresponding neural network model, as well as the parameter settings for each experiment. We also provide details about the dynamic DP-SGD federated learning algorithm for the corresponding federated learning experiments.

Benchmarks: We compare our proposed dynamic DP-SGD, growing- μ_t method, and sensitivity-decay method to the four benchmarks listed below.

(i) *SGD without DP:* The SGD method serve as the upper bound of model accuracy in the absence of clipping and additive noise. For the IMDB data set, we apply the Adam to compute the performance upper bound.

(ii) *Vanilla DP-SGD :* Under the same privacy budget constraint, Vannilla DP-SGD could require different amount of noise due to different DP accounting methods. It is shown by (Gopi et al., 2021) that the GDP CLT provides a tighter composition bound for DP-SGD and even underestimate the privacy cost compared to other methods including the

moment accountant method (Abadi et al., 2016). As a result, the calibrated noise power is lower than that obtained by moment accountant, resulting in a higher accuracy. Thereby, it provides the best performance that the vanilla DP-SGD can achieve with a predefined privacy budget. We therefore have vanilla DP-SGD under the privacy accounting by GDP CLT to sever as a baseline.

(iii) ρ -zCDP-SGD (Yu et al., 2019): This paper is relevant to our work as it proposes decaying the noise power during the SGD and computing the privacy loss using the ρ -zCDP. However, only parallel composition is considered, with no regard for DP amplification by subsampling.

(iv) tCDP-SGD (Zhang et al., 2021a): This more recently work proposed decaying the noise power for DP-SGD training as well as analyzing the DP composition and subsampling amplification under the truncated concentrated differential privacy (tCDP) framework.

Parameters: We concentrate on the strong privacy guarantee, with the smallest ϵ set to be 0.1. We set different ϵ 's denoted in each table due to different training data sizes and learning problem hardness; and $\delta = 1/(10|X|)$, where $|X|$ is the training data sample size. It is worth noting that we observed a significant performance degradation of DP-SGD when performing IMDB tasks. As a result, we also test a relatively large range of ϵ , i.e. $\epsilon \in [0.5, 9]$. The hyperparameters ρ_c and ρ_μ are swept in the following predefined sets: $1/\rho_c, 1/\rho_\mu \in \{0.1, 0.2, 0.3, 0.4, 0.5, 0.6, 0.7, 0.8\}$. Other hyper-parameters are detailed in Appendix A.9².

4.2. Results Analysis

Experiment results for the above six different datasets on MLP, CNN, LSTM, Federated Learning, and VGG models are shown in Table 1-Table 5, along with the performance of benchmarks and proposed methods. In general, the proposed extended GDP CLT supports the privacy accounting for dynamic clipping and noise power decay in dyamic DP-SGD. Separate experiments are carried out with the proposed growing- μ_t method, sensitivity-decay method, and dynamic DP-SGD method. The results in Table 1-Table 5 show consistently that all the three proposed methods improve performance when compared to the static noise GDP method (Bu et al., 2020). In particular, μ_t grows at the expense of early convergence speed in order to achieve higher accuracy, while sensitivity decay ensures more stable convergence. This explains why the sensitivity decay outperforms that of growing- μ_t . The dynamic DP-SGD, a combination of the two, improves performance while causing no additional privacy loss, as demonstrated by the Dynamic DP results in each table.

Specifically, experiments with different privacy budgets

²The code will be available shortly at github.com/dynamic-dp.

were conducted, and the results show that the stronger the privacy protection required (i.e., the lower ϵ value), the better the proposed dynamic DP-SGD method performs. For example, when $\epsilon = 0.4$ for the MNIST, (Yu et al., 2019) and (Zhang et al., 2021b) adopt noise decay, but their model fails to learn due to large calibrated noise power by the loose DP compositions. Our method, on the other hand, outperforms the vanilla DP-SGD method by a large margin, achieving 3.17% when $\epsilon = 0.4$ and even 4.6% for the LSTM network on NAME ($\epsilon = 1$) shown in Table 3.

It is worth noting that if the DP accountant is not tight enough, the noise power required will be overestimated, resulting in the noise dominating the gradient and causing the network to fail to learn. For example, the ρ -zCDP-SGD method with loose DP compositions performs significantly worse in the high privacy guarantee region due to overestimated noise. As a result, we only replicate its CNN model results on the MNIST and FashionMNIST datasets in Table 1, but omitting the meaningless results on other datasets. The extended GDP CLT, on the other hand, provides a detailed examination of DP amplification through subsampling as well as DP composition. As a result, for the same privacy budget, more precise noise power is calibrated.

4.3. Hyper-parameter sensitivity

We then test the robustness of dynamic DP-SGD performance to different values of ρ_μ and ρ_c as shown in Fig. 3. We use grid search to demonstrate the impact of these parameters on model performance. The dynamic method can consistently improve model performance across a wide range.

4.4. Exact Privacy Cost

Though (Dong et al., 2019) has shown that the GDP CLT approximate the true privacy cost with negligible error, Gopi et al. (2021) recently discovers that the GDP CLT may underestimate the privacy cost. The RDP accountant (Wang et al., 2019), on the other hand, overestimates the true cost. To evaluate the exact privacy cost, we plot the privacy cost curves for both the proposed extended GDP CLT and RDP in Fig. 4. Specifically, we set a target training round and conduct privacy accounting for the dynamic DP-SGD, based on the extended GDP CLT as well as RDP³ (Balle et al., 2020). Consequently, the true privacy cost curve must lie somewhere between these two limits. The result of extended GDP CLT is reasonable because the privacy cost differences between these two limits are small, particularly in the high privacy protection region.

It is worth noting that exact accounting can be performed using the recently proposed methods by (Gopi et al., 2021) and (Zhu et al., 2021), separately. However, because they

³For RDP, we use autodp library by (Wang) for DP accounting.

both require numerical computation, given a total privacy budget, the computation of different noise power for the mechanism of each step becomes much involved.

Table 1. CNN on MNIST and FashionMNIST datasets.

DP Accountant	Dynamic Noise	MNIST			FashionMNIST		
		$\epsilon = 0.4$	$\epsilon = 0.6$	$\epsilon = 1.2$	$\epsilon = 0.4$	$\epsilon = 1.2$	$\epsilon = 2.0$
Non-private	-	98.83			87.92		
ρ -zCDP-SGD	Noise Decay	10.28	10.12	65.33	9.86	63.30	72.18
tCDP-SGD	Noise Decay	26.93	83.28	92.60	53.69	76.48	77.58
Vanilla DP-SGD	-	91.18	93.80	95.50	76.77	80.45	82.55
Ours	Growing- μ_t	91.67	94.49	96.06	77.81	80.95	83.10
	Sensitivity Decay	93.95	95.17	96.17	78.11	82.83	83.64
	Dynamic DP	94.35	95.21	96.34	78.50	83.22	83.81

Table 2. MLP on the IMDB dataset.

DP Accountant	Dynamic Noise	IMDB				
		$\epsilon = 0.5$	$\epsilon = 1$	$\epsilon = 3$	$\epsilon = 6$	$\epsilon = 9$
Non-private	-	82.85				
tCDP-SGD	Noise Decay	56.67	58.24	62.15	65.88	70.16
Vanilla DP-SGD	-	63.62	69.71	75.64	77.75	78.60
Ours	Growing- μ_t	64.92	69.85	76.00	78.16	78.56
	Sensitivity Decay	65.44	70.25	76.23	78.47	79.42
	Dynamic GDP	65.63	70.77	76.64	78.61	79.61

Table 3. LSTM on NAME dataset.

DP Framework	Dynamic Noise	NAME			
		$\epsilon = 1$	$\epsilon = 2$	$\epsilon = 4$	$\epsilon = 8$
Non-private	-	80.14			
tCDP-SGD	Noise Decay	48.13	51.20	57.67	68.53
Vanilla DP-SGD	-	62.71	69.64	73.04	74.15
Extended CLT for GDP (Ours)	growing- μ_t	64.10	71.25	74.68	75.50
	Sensitivity Decay	66.66	71.78	73.67	74.78
	Dynamic DP	67.30	72.01	75.03	75.75

Table 4. Federated learning on InfiniteMNIST dataset.

DP Framework	Dynamic Noise	MNIST-250K			MNIST-500K		
		$\epsilon = 0.1$	$\epsilon = 0.4$	$\epsilon = 1$	$\epsilon = 0.1$	$\epsilon = 0.4$	$\epsilon = 1$
Non-private	-	98.89			98.96		
Vanilla DP-SGD	-	93.47	95.71	96.02	94.82	96.55	96.89
Ours	growing- μ_t	93.75	95.93	96.13	95.65	96.76	97.05
	Sensitivity Decay	94.46	95.90	96.40	95.75	96.83	97.06
	Dynamic DP	94.72	96.00	96.55	95.88	96.95	97.22

Table 5. VGG-11 on chest radiographs.

DP Framework	Dynamic Noise	Chest Xray		
		$\epsilon = 0.5$	$\epsilon = 1$	$\epsilon = 1.5$
Non-private	-	97.02		
Vanilla DP-SGD	-	92.24	93.18	93.44
Ours	growing- μ_t	92.60	93.65	94.01
	Sensitivity Decay	92.89	93.78	94.24
	Dynamic DP	93.30	94.01	94.43

5. Theoretical Analysis

In this section, we theoretically examine the impact of varying DP costs on DP-SGD utility guarantees. To begin with, we state a general form of dynamic DP-SGD where C_t and σ_t can be arbitrary predefined sequences in Algorithm 3. Compared with Algorithm 2, aside from allowing

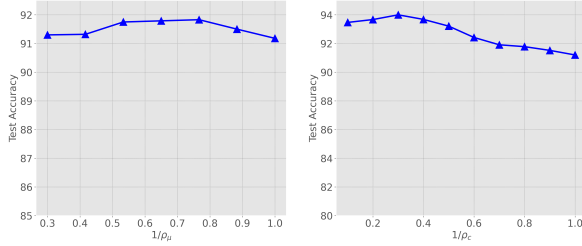


Figure 3. Dynamic DP-SGD performance is robust to ρ_μ and ρ_c .

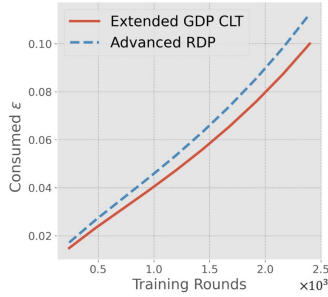


Figure 4. Upper bound (advanced RDP) and lower bound (extended GDP CLT) of the dynamic DP-SGD privacy cost curves. The true privacy cost must lie somewhere between these two limits. The result of extended CLT for GDP is reasonable because the privacy cost differences between these two limits are small, especially in the high privacy protection region.

arbitrary sequences C_0, C_1, \dots, C_T and $\sigma_1, \sigma_2, \dots, \sigma_T$, we denote $\sigma_t = \tilde{\sigma} \cdot \tilde{\sigma}_t$ for the convenience of analysis. Besides, in step 3 of Algorithm 3, we use $p|X|$ to replace $|X_t|$ with the intuition being $\mathbb{E}[|X_t|] = p|X|$, where p is the sampling rate. Such a replacement can also be found in Abadi et al. (2016), which is one of the most well-known version of DP-SGD. The main advantage of this form in our situation is that it simplifies the utility analysis by removing the need to calculate the first and second moments of $\frac{1}{|X_t|}$, which take complicated forms. To proceed with utility analysis, we first state a corollary of Theorem 1 regarding the requirement of $\tilde{\sigma}$ with proof provided in Appendix A.5.

Corollary 2. Algorithm 3 satisfies $G_{\mu_{\text{tot}}}$ -DP if

$$\tilde{\sigma} = p \frac{1}{\mu_{\text{tot}}} \sqrt{2 \sum_{t=1}^T \frac{C_t^2}{\tilde{\sigma}_t^2}}, \quad (15)$$

and $\frac{C_t}{\tilde{\sigma}_t} \leq 1, \forall t \in [T]$.

Corollary 2 is a direct implication of Theorem 1 with a mild constraint $\frac{C_t}{\tilde{\sigma}_t} = \mu_t \leq 1$. Note that $\mu_t \leq 1$ is guaranteed for strong privacy as $\mu_t \ll \mu_{\text{tot}}$, and $\mu_{\text{tot}} = 1$ is just borderline private pointed out by Dong et al. (2019). The smaller μ_{tot} , the more privacy it preserves.

Denote the objective function as $L(\theta) = \frac{1}{N} \sum_{i=1}^N f(\theta, x_i)$ and the clipped stochastic gradient at step t as $g_t =$

Algorithm 3 General Dynamic DP-SGD Algorithm

Require: DP budget (ϵ, δ) , sampling rate p , clipping threshold C_1, \dots, C_T , and noise power $\tilde{\sigma} \cdot \tilde{\sigma}_1, \tilde{\sigma} \cdot \tilde{\sigma}_2, \dots, \tilde{\sigma} \cdot \tilde{\sigma}_T$.

- 1: **for** $t = 1, \dots, T$ **do**
- 2: Sample $X_t \in X$ with sampling rate p and sample noise $\xi_t \sim \mathcal{N}(0, \tilde{\sigma}^2 I)$.
- 3: Compute: $\theta_{t+1} = \theta_t - \frac{\eta}{p|X|} [\sigma_t \xi_t + \sum_{x \in X_t} \text{CL}(g_x; C_t)]$ with $\text{CL}(\cdot)$ in (3)
- 4: **end for**

$\frac{1}{p|X|} [\sum_{x \in X_t} \text{CL}(g_x; C_t)]$ where $g_x \triangleq \frac{\partial f(\theta_t, x)}{\partial \theta_t}$. Assume function $L(\theta)$ is Q -smooth, i.e., $L(\theta') - L(\theta) \leq \langle \nabla L(\theta), \theta' - \theta \rangle + \frac{Q}{2} \|\theta - \theta'\|^2$, and each per-sample gradient is upper-bounded, i.e. $\|g_x\| \leq G$. We prove the following theorem to show the privacy-utility trade-off of Algorithm 3 with details in Appendix A.6.

Theorem 1. The dynamic DP-SGD (Algorithm 3) satisfies the following utility guarantee

$$\begin{aligned} & \mathbb{E} \left[\frac{1}{T} \sum_{t=1}^T \|\nabla L(\theta_t)\|^2 \right] \\ & \leq \frac{1}{\eta T} \mathbb{E}[L(\theta_1) - L(\theta_{T+1})] + \frac{Q}{2} \frac{\eta}{T} \sum_{t=1}^T \mathbb{E}[\|g_t\|^2] \\ & + \underbrace{\mathbb{E} \left[\frac{1}{T} \sum_{t=1}^T \|\nabla L(\theta_t)\| P_t(C_t) G \right]}_{\triangleq \text{bias term}} + \frac{Q}{2} \frac{\eta}{p^2 N^2} \underbrace{\frac{1}{T} \sum_{t=1}^T \tilde{\sigma}^2 \tilde{\sigma}_t^2}_{\triangleq D_1}, \end{aligned} \quad (16)$$

where $P_t(C_t)$ is the probability of a per-sample gradient being clipped with threshold C_t at θ_t , and the expectations are taken over all randomness including gradient sampling and noise sampling. Assume $\sigma_t = \Theta(1)$ and $C_t = \Theta(1)$, after setting $\eta T = N \mu_{\text{tot}}$, $\eta = \frac{1}{N \mu_{\text{tot}}}$, and substituting $\tilde{\sigma}$ from Corollary 2 into Eq. (16), we have

$$\mathbb{E} \left[\frac{1}{T} \sum_{t=1}^T \|\nabla L(\theta_t)\|^2 \right] = O \left(\frac{1}{N \mu_{\text{tot}}} \right) + \text{bias term}.$$

Remark on convergence rate: The derived convergence rate is $O(1/(N \mu_{\text{tot}}))$ ignoring the non-vanishing bias term. This rate is in the same polynomial order as existing analyses, e.g., $\tilde{O}(1/(N \epsilon))$ rate in Theorem 5 of Zhang et al. (2017). The non-vanishing bias term caused by gradient clipping is unavoidable since it is proven in Song et al. (2020) that DP-SGD with clipping suffers a constant regret in the worst case. A similar bound is also observed in Chen et al. (2020), in which the impact of gradient clipping on symmetric gradient distributions is studied. The difference is that our bound is based on Gaussian DP and the bias term is expressed in a simpler form applicable for arbitrary distributions. As will be evident later, this simpler form provides

intuitions on why clipping threshold and noise should be adjusted dynamically.

Remark on gradient clipping C_t : The clipping operation will cause estimation bias of the true gradient, which could lead to a constant regret for the algorithm. This fact is reflected by the *bias* term on the r.h.s. of (16). And it can be seen from $P_t(C_t)$ (defined as the probability of a per-sample gradient being clipped with threshold C_t at θ_t) that in general, the *bias* term will be small if C_t 's are large and vice versa, given the same distribution of gradients. This means that if we use large clipping thresholds, we will reduce the *bias* term, but at the expense of a larger D_1 as indicated by Corollary 2 and (16). Thus, one should choose a sequence of C_t that could better balance the bias term and the variance term D_1 . However, an optimal solution requires knowing the distribution of the stochastic gradient which is nearly impossible in practice. Choosing C_t is more of an art than a science, according to the existing literature. One notable practical good choice is to keep $P_t(C_t)$ roughly constant, as proposed in (Andrew et al., 2021). Under situations when the gradients are decreasing across iterations, this choice implies C_t should be decreasing to keep $P_t(C_t)$ a constant (see Figure 4 in (Andrew et al., 2021)). This supports the sensitivity decay method in our Algorithm 2.

Remark on term D_1 : The first two terms on the RHS of (16) are standard in SGD analysis. We now focus on the term D_1 caused by privacy noise, which becomes

$$p^2 \frac{2}{\mu_{\text{tot}}^2} \frac{1}{T} \sum_{t=1}^T \tilde{\sigma}_t^2 \sum_{t=1}^T \frac{C_t^2}{\tilde{\sigma}_t^2} \quad (17)$$

after substituting $\tilde{\sigma}$ from Corollary 2. One can readily notice that given the sequence of C_t , this term can be minimized by choosing $\tilde{\sigma}_t$. This problem also appeared in Pichapati et al. (2019) and Wu et al. (2021). It turns out that minimizing (17) w.r.t the sequence σ_t admits an optimal solution $\tilde{\sigma}_t = \sqrt{C_t}$ (see Appendix A.7 for proof). Combining with the fact that $\mu_t = \frac{C_t}{\tilde{\sigma}_t \sigma}$ indicates $\mu_t \propto \sqrt{C_t}$, which gives a theoretical way to allocate noise given a sequence of clipping thresholds and support that we should change μ_t in different iterations. Yet, this particular choice of σ_t is based on the very simplified assumption that may not reflect the whole picture of training neural nets. For example, it is widely known that the loss of training neural nets usually have different curvatures across different regions reachable by different iterations. If we take into this consideration and replace the Q-smooth assumption by $\mathbb{E}[L(\theta_{t+1})] - L(\theta) \leq \langle \nabla L(\theta_t), \mathbb{E}[\theta_{t+1} - \theta_t] \rangle + \frac{Q_t}{2} \mathbb{E}[\|\theta_{t+1} - \theta_t\|^2]$ in Theorem 1, we will reach a conclusion that $\sigma_t = \sqrt{C_t} Q_t^{1/4}$, which indicates the allocation of privacy noise should also consider the local curvature in different iterations unknown before training (see Appendix A.8 for a detailed statement and proof). We thus believe that a good choice of σ_t and C_t should be

based more on empirical performance of a particular choice, like the one provided in Section 4. Meanwhile, we hope our theoretical analysis can provide some insights about understanding this problem and inspire future explorations.

6. Related Work

DP-SGD Algorithm To improve the model's accuracy, previous work has concentrated on designing variations of DP-SGD by estimating the clipping bound and minimizing the bias introduced by gradient clipping. More precisely, Abadi et al. (2016) propose norm clipping and per-layer clipping, both of which select clipping values based on gradient differences between different layers. Pichapati et al. (2019) study AdaClip, a coordinate-wise clipping method that could reduce the total amount of noise required. Thakkar et al. (2019) introduce gradient clipping based on the quantile statistics of the gradient, which requires additional DP cost to protect those quantiles. Recently, Chen et al. (2020) analyze the bias introduced by the gradient clipping operation and propose a method for reducing the bias error by first adding noise before clipping. In the meantime of this paper, Wu et al. (2021) propose adaptive DP version of SGD where the random noise added to the gradient is optimally adapted to the stepsize. This method, however, is inapplicable for those with stepsizes that being updated on the fly, such as AdaGrad and Adam, as stated in the paper. It's worth noting that the proposed dynamic DP-SGD in this paper is compatible with the methods in Thakkar et al. (2019); Chen et al. (2020); Wu et al. (2021) and can be used in tandem to investigate accuracy improvement but involve more details and is one potential avenue of future work.

Furthermore, Yu et al. (2019) provide a means of reducing noise variance during the DP-SGD process, thereby improving model performance; and Zhang et al. (2021b) analyze the DP cost for the same method using the z-CDP privacy accounting. Due to the loose DP accountings, these methods have a large performance gap in the high privacy guaranteed region. As demonstrated in the experiments, the proposed dynamic DP-SGD improves these results significantly due to the dynamic clipping operation and tight DP composition. Recently, Zhou et al. (2020); He et al. study the relationships between generalization and privacy private learning algorithm.

7. Conclusions

In this paper, we have developed the dynamic differentially-private stochastic gradient descent (dynamic DP-SGD) optimizer, which has varying clipping values and noise powers across the update. The dynamic privacy cost is tightly accounted by the extended central limit theorem of Gaussian differential privacy, allowing dynamic noise to be calibrated

for each individual training step within a predefined privacy budget. In contrast to the vanilla DP-SGD, we are able to reduce the noise term in the utility upper bound without compromising privacy as the insight gained according to our theoretical analysis. Extensive testing on a variety of datasets and models demonstrates that the dynamic DP-SGD consistently and clearly outperforms existing methods especially in the strong privacy region.

ACKNOWLEDGMENTS

We would like to thank Yuxiang Wang for his helpful discussion.

References

- Martín Abadi, Andy Chu, Ian J. Goodfellow, H. Brendan McMahan, Ilya Mironov, Kunal Talwar, and Li Zhang. Deep learning with differential privacy. In Edgar R. Weippl, Stefan Katzenbeisser, Christopher Kruegel, Andrew C. Myers, and Shai Halevi (eds.), *Proceedings of the 2016 ACM SIGSAC Conference on Computer and Communications Security, Vienna, Austria, October 24-28, 2016*, pp. 308–318. ACM, 2016.
- Galen Andrew, Om Thakkar, H Brendan McMahan, and Swaroop Ramaswamy. Differentially private learning with adaptive clipping. *Advances in Neural Information Processing Systems 34 pre-proceedings*, 2021.
- Borja Balle, Gilles Barthe, and Marco Gaboardi. Privacy profiles and amplification by subsampling. *Journal of Privacy and Confidentiality*, 10(1), 2020.
- Léon Bottou, Frank E Curtis, and Jorge Nocedal. Optimization methods for large-scale machine learning. *Siam Review*, 60(2):223–311, 2018.
- Zhiqi Bu, Jinshuo Dong, Qi Long, and Weijie J. Su. Deep learning with Gaussian differential privacy. *Harvard data science review*, 2020 23, 2020.
- Xiangyi Chen, Zhiwei Steven Wu, and Mingyi Hong. Understanding gradient clipping in private SGD: A geometric perspective. In Hugo Larochelle, Marc’Aurelio Ranzato, Raia Hadsell, Maria-Florina Balcan, and Hsuan-Tien Lin (eds.), *Advances in Neural Information Processing Systems 33: Annual Conference on Neural Information Processing Systems 2020, NeurIPS 2020, December 6-12, 2020, virtual*, 2020.
- Jinshuo Dong, Aaron Roth, and Weijie J Su. Gaussian differential privacy. *arXiv preprint arXiv:1905.02383*, 2019.
- Cynthia Dwork. Differential privacy. In Michele Bugliesi, Bart Preneel, Vladimiro Sassone, and Ingo Wegener (eds.), *Automata, Languages and Programming, 33rd International Colloquium, ICALP 2006, Venice, Italy, July 10-14, 2006, Proceedings, Part II*, volume 4052 of *Lecture Notes in Computer Science*, pp. 1–12. Springer, 2006.
- Cynthia Dwork, Aaron Roth, et al. The algorithmic foundations of differential privacy. *Found. Trends Theor. Comput. Sci.*, 9(3-4):211–407, 2014.
- Sivakanth Gopi, Yin Tat Lee, and Lukas Wutschitz. Numerical composition of differential privacy. *arXiv preprint arXiv:2106.02848*, 2021.
- Fengxiang He, Bohan Wang, and Dacheng Tao. Tighter generalization bounds for iterative privacy-preserving algorithms. In *the 37th Conference on Uncertainty in Artificial Intelligence (UAI 2021)*.
- Daniel S Kermany, Michael Goldbaum, Wenjia Cai, Carolina CS Valentim, Huiying Liang, Sally L Baxter, Alex McKeown, Ge Yang, Xiaokang Wu, Fangbing Yan, et al. Identifying medical diagnoses and treatable diseases by image-based deep learning. *Cell*, 172(5):1122–1131, 2018.
- Y. Lecun and L. Bottou. Gradient-based learning applied to document recognition. *Proceedings of the IEEE*, 86(11): 2278–2324, 1998.
- Venkatadheeraj Pichapati, Ananda Theertha Suresh, Felix X. Yu, Sashank J. Reddi, and Sanjiv Kumar. Adaclip: Adaptive clipping for private sgd. *ArXiv*, abs/1908.07643, 2019.
- Shuang Song, Om Thakkar, and Abhradeep Thakurta. Characterizing private clipped gradient descent on convex generalized linear problems. *arXiv preprint arXiv:2006.06783*, 2020.
- Om Thakkar, Galen Andrew, and H. Brendan McMahan. Differentially private learning with adaptive clipping. *CoRR*, abs/1905.03871, 2019.
- Yu-Xiang Wang, Borja Balle, and Shiva Prasad Kasiviswanathan. Subsampled Rényi differential privacy and analytical moments accountant. In *The 22nd International Conference on Artificial Intelligence and Statistics*, pp. 1226–1235. PMLR, 2019.
- Yuxiang Wang. autodp: A flexible and easy-to-use package for differential privacy. <https://github.com/yuxiangw/autodp>. Accessed: 2021-09-30.
- Xiaoxia Wu, Lingxiao Wang, Irina Cristali, Quanquan Gu, and Rebecca Willett. Adaptive differentially private empirical risk minimization. *arXiv preprint arXiv:2110.07435*, 2021.

Lei Yu, Ling Liu, Calton Pu, Mehmet Emre Gursoy, and Stacey Truex. Differentially private model publishing for deep learning. In *2019 IEEE Symposium on Security and Privacy (SP)*, pp. 332–349. IEEE, 2019.

Jiaqi Zhang, Kai Zheng, Wenlong Mou, and Liwei Wang. Efficient private erm for smooth objectives. *arXiv preprint arXiv:1703.09947*, 2017.

Xinyue Zhang, Jiahao Ding, Maoqiang Wu, Stephen T. C. Wong, Hien Van Nguyen, and Miao Pan. Adaptive privacy preserving deep learning algorithms for medical data. In *IEEE Winter Conference on Applications of Computer Vision, WACV 2021, Waikoloa, HI, USA, January 3-8, 2021*, pp. 1168–1177. IEEE, 2021a.

Xinyue Zhang, Jiahao Ding, Maoqiang Wu, Stephen TC Wong, Hien Van Nguyen, and Miao Pan. Adaptive privacy preserving deep learning algorithms for medical data. In *Proceedings of the IEEE/CVF Winter Conference on Applications of Computer Vision*, pp. 1169–1178, 2021b.

Bo Zhao, Konda Reddy Mopuri, and Hakan Bilen. idlg: Improved deep leakage from gradients. *ArXiv*, abs/2001.02610, 2020.

Yingxue Zhou, Xiangyi Chen, Mingyi Hong, Zhiwei Steven Wu, and Arindam Banerjee. Private stochastic non-convex optimization: Adaptive algorithms and tighter generalization bounds. *arXiv preprint arXiv:2006.13501*, 2020.

Ligeng Zhu and Song Han. Deep leakage from gradients. In Qiang Yang, Lixin Fan, and Han Yu (eds.), *Federated Learning - Privacy and Incentive*, volume 12500 of *Lecture Notes in Computer Science*, pp. 17–31. Springer, 2020.

Yuqing Zhu, Jinshuo Dong, and Yu-Xiang Wang. Optimal accounting of differential privacy via characteristic function. *arXiv preprint arXiv:2106.08567*, 2021.

Alexander Ziller, Dmitrii Usynin, Rickmer Braren, Marcus Makowski, Daniel Rueckert, and Georgios Kaissis. Medical imaging deep learning with differential privacy. *Scientific Reports*, 11(1):1–8, 2021.

A. Appendix

A.1. Unstable Updates

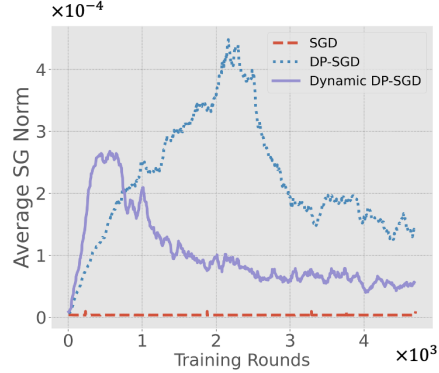


Figure 5. Experiments on Fashion-MNIST for both DP-SGD and the proposed dynamic DP-SGD with the same corresponding settings as that in Table 1. In comparison to SGD, DP-SGD is unstable, and the stochastic gradient (SG) norm has a ramp-up period. However, the SG norm is stabilized by the dynamic DP-SGD.

A.2. GDP Preliminary

We first introduce some background about GDP. Let P and Q denote the distributions of $M(X)$ and $M(X')$ with $X \sim X'$, and let ϕ be any (possibly randomized) rejection rule for testing $H_0 : P$ against $H_1 : Q$. With these in place, Dong et al. (2019) defines the trade-off function of P and Q as

$$\begin{aligned} T(P, Q) : [0, 1] &\mapsto [0, 1] \\ \alpha &\mapsto \inf_{\phi} \{1 - \mathbb{E}_Q[\phi] : \mathbb{E}_P[\phi] \leq \alpha\}. \end{aligned} \quad (18)$$

Above, $\mathbb{E}_P[\phi]$ and $1 - \mathbb{E}_Q[\phi]$ are type I and type II errors of the rejection rule ϕ , respectively. It is shown that $T(P, Q) \geq T(\mathcal{N}(0, 1), \mathcal{N}(\mu, 1)) \triangleq G_{\mu}$, which is referred to as μ -GDP.

In each step of the DP-SGD in (4) with the Gaussian mechanism, it achieves μ -GDP with $\mu = \frac{c}{\sigma}$. Consider the sampling scheme $\text{PS}(X)$ that each individual data sample (x, y) is subsampled independently with probability p from the training set to construct X_t . It is shown in (Bu et al., 2020) that given two neighboring datasets X and X' , if a randomized mechanism \mathcal{M} is G_{μ} -DP, then

$$T(\mathcal{M} \circ \text{PS}(X), \mathcal{M} \circ \text{PS}(X')) \geq pG_{\mu} + (1-p)\text{Id}, \quad (19)$$

where $\text{Id}(x) = 1 - x$. Then after a large enough T steps, a Berry-Esseen style CLT result is shown by (Bu et al., 2020) that as $T \rightarrow +\infty$ and $p\sqrt{T} \rightarrow$ a constant, the composition of the r.h.s. of (19) converges to a $G_{\mu_{\text{tot}}}$ -DP with

$$\mu_{\text{tot}} = p\sqrt{T(e^{\mu^2} - 1)}. \quad (20)$$

A.3. Proof of Theorem 1

Following the proof of f -DP central limit theorem in (Bu et al., 2020), we have the following definitions given a function f :

$$\text{kl}(f) \triangleq - \int_0^1 \log |f'(x)| dx, \quad (21)$$

$$\tilde{\text{kl}}(f) \triangleq \int_0^1 |f'(x)| \log |f'(x)| dx, \quad (22)$$

$$\kappa_2(f) \triangleq \int_0^1 \log^2 |f'(x)| dx, \quad (23)$$

$$\tilde{\kappa}_2(f) \triangleq \int_0^1 |f'(x)| \log^2 |f'(x)| dx, \quad (24)$$

$$\kappa_3(f) \triangleq \int_0^1 |\log |f'(x)||^3 dx, \quad (25)$$

$$\tilde{\kappa}_3(f) \triangleq \int_0^1 |f'(x)| \cdot |\log |f'(x)||^3 dx. \quad (26)$$

Let $\{f_{ni} : 1 \leq i \leq n\}_{n=1}^\infty$ be a triangular array of trade-off functions and assume the following limits for some constants $K \geq 0$ and $s > 0$ as $n \rightarrow \infty$:

1. $\sum_{i=1}^n \text{kl}(f_{ni}) + \tilde{\text{kl}}(f_{ni}) \rightarrow K$,
2. $\max_{1 \leq i \leq n} \text{kl}(f_{ni}) \rightarrow 0$, $\max_{1 \leq i \leq n} \tilde{\text{kl}}(f_{ni}) \rightarrow 0$,
3. $\sum_{i=1}^n \kappa_2(f_{ni}) \rightarrow s^2$, $\sum_{i=1}^n \tilde{\kappa}_2(f_{ni}) \rightarrow s^2$,
4. $\sum_{i=1}^n \kappa_3(f_{ni}) \rightarrow 0$, $\sum_{i=1}^n \tilde{\kappa}_3(f_{ni}) \rightarrow 0$,

it is shown in (Bu et al., 2020) that

$$\lim_{n \rightarrow \infty} f_{n1} \otimes f_{n2} \otimes \cdots \otimes f_{nn}(\alpha) = G_{K/s}(\alpha) \quad (27)$$

uniformly for all $\alpha \in [0, 1]$. Let $g_t(x) = -G'_{\mu_t} - 1 = |G'_{\mu_t}| - 1$, where the second equation is due to the definition of the tradeoff function. Then by replacing n by t , equations from (21) to (26) are reformulated as:

$$\text{kl}(f_{p,t}) = - \int_0^1 \log(1 + pg_t(x)) dx, \quad (28)$$

$$\tilde{\text{kl}}(f_{p,t}) = \int_0^1 (1 + pg_t(x)) \log(1 + pg_t(x)) dx, \quad (29)$$

$$\kappa_2(f_{p,t}) = \int_0^1 [\log(1 + pg_t(x))]^2 dx, \quad (30)$$

$$\tilde{\kappa}_2(f_{p,t}) = \int_0^1 (1 + pg_t(x)) [\log(1 + pg_t(x))]^2 dx, \quad (31)$$

$$\kappa_3(f_{p,t}) = \int_0^1 [\log(1 + pg_t(x))]^3 dx, \quad (32)$$

$$\tilde{\kappa}_3(f_{p,t}) = \int_0^1 (1 + pg_t(x)) [\log(1 + pg_t(x))]^3 dx. \quad (33)$$

According to (27), we need to compute $\sum_{t=1}^T (\text{kl}(f_{p,t}) + \tilde{\text{kl}}(f_{p,t}))$ and $\sum_{t=1}^T \kappa_2(f_{p,t})$ to obtain the CLT. Let $p\sqrt{T} \rightarrow v$ and $p \rightarrow 0^+$, we compute K by

$$\begin{aligned} K &= \lim_{\substack{p \rightarrow 0^+ \\ p\sqrt{T} \rightarrow v}} \sum_{t=1}^T (\text{kl}(f_{p,t}) + \tilde{\text{kl}}(f_{p,t})) \\ &= \lim_{\substack{p \rightarrow 0^+ \\ p\sqrt{T} \rightarrow v}} \sum_{t=1}^T p \int_0^1 g_t(x) \cdot \log(1 + pg_t(x)) dx \\ &= \sum_{t=1}^T \int_0^1 \frac{v^2}{T} \cdot g_t(x) \cdot \lim_{p \rightarrow 0^+} \frac{1}{p} \log(1 + pg_t(x)) dx \\ &= \frac{v^2}{T} \sum_{t=1}^T \int_0^1 g_t(x)^2 dx \\ &= \frac{v^2}{T} \sum_{t=1}^T (e^{\mu_t^2} - 1). \end{aligned} \quad (34)$$

We further compute s following the same procedure:

$$\begin{aligned} s^2 &= \sum_{t=1}^T \kappa_2(f_{p,t}) \\ &= \frac{v^2}{T} \sum_{t=1}^T \int_0^1 \lim_{p \rightarrow 0^+} \left[\frac{1}{p} \log(1 + pg_t(x)) \right]^2 dx \\ &= \frac{v^2}{T} \sum_{t=1}^T \int_0^1 g_t(x)^2 dx \\ &= \frac{v^2}{T} \sum_{t=1}^T (e^{\mu_t^2} - 1). \end{aligned} \quad (35)$$

Substituting (34) and (35) into (27), we have

$$\lim_{T \rightarrow \infty} f_{p,t} \otimes_{t=1}^T = G_\mu \quad (36)$$

with

$$\mu = \frac{K}{s} = p \sqrt{\sum_{t=1}^T (e^{\mu_t^2} - 1)}. \quad (37)$$

A.4. Dynamic DP-Adam

Algorithm 4 Dynamic DP-Adam Algorithm

Require: DP budget (ϵ, δ) , sampling rate p , momentum parameters (β_1, β_2) , a small constant $z > 0$, and hyper-parameters: ρ_μ, ρ_c and C_0 .

- 1: Compute μ_0 in Algorithm 1
 - 2: **for** $t = 1, \dots, T$ **do**
 - 3: Compute $C_t = (\rho_c)^{-\frac{t}{T}} \cdot C_0$ in (12)
 - 4: Calibrate noise : $\sigma_t = \frac{C_0}{\mu_0} (\rho_\mu \cdot \rho_c)^{-\frac{t}{T}}$
 - 5: Sample $X_t \in X$ with sampling rate p and sample noise $\xi_t \sim \mathcal{N}(0, \sigma_t^2 I)$.
 - 6: Compute: $\tilde{g}_t = \frac{1}{|X_t|} [\xi_t + \sum_{x \in X_t} \text{CL}(g_x; C_t)]$ with $\text{CL}(\cdot)$ in (3)
 - 7: Compute biased first momentum: $m_t = \beta_1 m_{t-1} + (1 - \beta_1) \tilde{g}_t$
 - 8: Compute biased second momentum: $u_t \leftarrow \beta_2 u_{t-1} + (1 - \beta_2) (\tilde{g}_t \odot \tilde{g}_t)$
 - 9: Compute bias-corrected first moment: $\hat{m}_t = m_t / (1 - \beta_1^t)$
 - 10: Compute bias-corrected second moment $\hat{v}_t = v_t / (1 - \beta_2^t)$
 - 11: Compute: $w_t = \hat{m}_t / (\sqrt{\hat{v}_t} + z)$
 - 12: Compute: $\theta_{t+1} = \theta_t - \eta w_t$
 - 13: **end for**
-

A.5. Proof of Corollary 2

From the definition Gaussian DP in Eq.(2), we know each step in Algorithm 3 is G_{μ_t} -DP and

$$\mu_t = \frac{C_t}{\tilde{\sigma}_t \tilde{\sigma}}. \quad (38)$$

Further, by Theorem 1, we know overall Algorithm 3 is G_μ -DP with

$$\mu = p \sqrt{\sum_{t=1}^T (e^{\mu_t^2} - 1)}. \quad (39)$$

Because $e^x < 1 + 2x$ for $0 \leq x \leq 1$, we know

$$\mu < p \sqrt{2 \sum_{t=1}^T \mu_t^2}, \quad \text{when } \mu_t^2 \leq 1. \quad (40)$$

Given a total privacy budget μ_{tot} that bounds the above μ , we have

$$\mu < p \sqrt{2 \sum_{t=1}^T \mu_t^2} = p \sqrt{2 \sum_{t=1}^T \frac{C_t^2}{\tilde{\sigma}_t^2 \tilde{\sigma}^2}} \leq \mu_{\text{tot}}. \quad (41)$$

Rearranging the last inequality, we get

$$\tilde{\sigma} \geq p \frac{1}{\mu_{\text{tot}}} \sqrt{2 \sum_{t=1}^T \frac{C_t^2}{\tilde{\sigma}_t^2}}, \quad (42)$$

which is sufficient to guarantee Algorithm 3 to satisfy $G_{\mu_{\text{tot}}}$ -DP.

A.6. Proof of Theorem 1

By the update rule in Algorithm 3, we know

$$\theta_{t+1} = \theta_t - \frac{\eta}{pN} \tilde{\sigma}_t \xi_t - \eta g_t. \quad (43)$$

By the assumption that the objective function $L(\cdot)$ is Q -smooth, we have

$$\begin{aligned} \mathbb{E}_t[L(\theta_{t+1})] &\leq L(\theta_t) + \mathbb{E}_t[\langle \nabla L(\theta_t), (\theta_{t+1} - \theta_t) \rangle] \\ &\quad + \mathbb{E}_t\left[\frac{Q}{2} \|\theta_{t+1} - \theta_t\|^2\right] \\ &\leq L(\theta_t) - \eta \langle \nabla L(\theta_t), \mathbb{E}_t[g_t] \rangle + \frac{Q}{2} \eta^2 \mathbb{E}_t[\|g_t\|^2] \\ &\quad + \frac{Q}{2} \frac{\eta^2}{N^2 p^2} \tilde{\sigma}_t^2 \tilde{\sigma}_t^2, \end{aligned} \quad (44)$$

where \mathbb{E}_t denotes expectation taken over randomness at step t , including gradient sampling and noise sampling. Taking the sum of t from 1 to T and the expectation of all steps, we get

$$\begin{aligned} &\mathbb{E}[L(\theta_{T+1})] - \mathbb{E}[L(\theta_1)] \\ &\leq -\eta \mathbb{E}\left[\sum_{t=1}^T \langle \nabla L(\theta_t), \mathbb{E}_t[g_t] \rangle\right] + \frac{Q}{2} \eta^2 \sum_{t=1}^T \mathbb{E}[\|g_t\|^2] \\ &\quad + \sum_{t=1}^T \frac{Q}{2} \frac{\eta^2}{N^2 p^2} \tilde{\sigma}_t^2 \tilde{\sigma}_t^2. \end{aligned} \quad (45)$$

Rearranging and dividing both sides by $T\eta$, we have

$$\begin{aligned} &\frac{1}{T} \mathbb{E}\left[\sum_{t=1}^T \langle \nabla L(\theta_t), \mathbb{E}_t[g_t] \rangle\right] \\ &\leq \frac{1}{\eta T} (\mathbb{E}[L(\theta_1)] - \mathbb{E}[L(\theta_{T+1})]) + \frac{1}{T} \frac{Q}{2} \eta \sum_{t=1}^T \mathbb{E}[\|g_t\|^2] \\ &\quad + \frac{1}{T} \sum_{t=1}^T \frac{Q}{2} \frac{\eta}{N^2 p^2} \tilde{\sigma}_t^2 \tilde{\sigma}_t^2. \end{aligned} \quad (46)$$

Further, we know

$$\begin{aligned}
 \mathbb{E}_t[g_t] &= \mathbb{E}\left[\frac{1}{p|X|} \left[\sum_{x \in X_t} \text{CL}(g_x; C_t) \right]\right] \\
 &= \mathbb{E}_{X_t} \left[\frac{1}{p|X|} \left[\sum_{x \in X_t} \text{CL}(g_x; C_t) \right]\right] \\
 &\stackrel{(i)}{=} \frac{1}{p|X|} p|X| \mathbb{E}_x[\text{CL}(g_x; C_t)] \\
 &\stackrel{(ii)}{=} \sum_{i=1}^N \frac{1}{N} \text{CL}(g_{x_i}; C_t) \\
 &\stackrel{(iii)}{=} \sum_{i=1}^N \frac{1}{N} \mathbb{1}[\|g_{x_i}\| \leq C_t] g_{x_i} \\
 &\quad + \sum_{i=1}^N \frac{1}{N} \mathbb{1}[\|g_{x_i}\| > C_t] g_{x_i} \frac{C_t}{\|g_{x_i}\|} \\
 &= \sum_{i=1}^N \frac{1}{N} g_{x_i} \\
 &\quad + \sum_{i=1}^N \frac{1}{N} \mathbb{1}[\|g_{x_i}\| > C_t] g_{x_i} \left(\frac{C_t}{\|g_{x_i}\|} - 1 \right),
 \end{aligned} \tag{47}$$

where (i) is due to each element in X has p probability being in X_t and \mathbb{E}_x is taken over a uniform distribution of $x \in X$; (ii) is because we assumed that there is N samples of x ; (iii) is due to the definition of clipping operation.

Recall the fact that $\nabla L(\theta_t) = \frac{1}{N} \sum_{i=1}^N g_{x_i}$ and the assumption $\|g_{x_i}\| \leq G$, we have

$$\begin{aligned}
 &\|\mathbb{E}_t[g_t] - \nabla L(\theta_t)\| \\
 &= \left\| \sum_{i=1}^N \frac{1}{N} \mathbb{1}[\|g_{x_i}\| > C_t] g_{x_i} \left(\frac{C_t}{\|g_{x_i}\|} - 1 \right) \right\| \\
 &\leq \sum_{i=1}^N \frac{1}{N} \mathbb{1}[\|g_{x_i}\| > C_t] G \\
 &= P_t(C_t)G,
 \end{aligned} \tag{48}$$

where $P_t(C_t)$ denotes the probability of a per-sample gradient being clipped at step t given θ_t and X .

Then we know

$$\begin{aligned}
 &\frac{1}{T} \mathbb{E} \left[\sum_{t=1}^T \langle \nabla L(\theta_t), \mathbb{E}_t[g_t] \rangle \right] \\
 &= \frac{1}{T} \mathbb{E} \left[\sum_{t=1}^T \langle \nabla L(\theta_t), \nabla L(\theta_t) - \nabla L(\theta_t) + \mathbb{E}_t[g_t] \rangle \right] \\
 &\geq \frac{1}{T} \mathbb{E} \left[\sum_{t=1}^T \|\nabla L(\theta_t)\|^2 \right] \\
 &\quad - \frac{1}{T} \mathbb{E} \left[\sum_{t=1}^T \|\nabla L(\theta_t)\| \|\nabla L(\theta_t) - \mathbb{E}_t[g_t]\| \right] \\
 &\geq \frac{1}{T} \mathbb{E} \left[\sum_{t=1}^T \|\nabla L(\theta_t)\|^2 \right] \\
 &\quad - \frac{1}{T} \mathbb{E} \left[\sum_{t=1}^T \|\nabla L(\theta_t)\| P_t(C_t)G \right].
 \end{aligned} \tag{49}$$

Substituting (49) into the LHS of (46), we get

$$\begin{aligned}
 &\frac{1}{T} \mathbb{E} \left[\sum_{t=1}^T \|\nabla L(\theta_t)\|^2 \right] \\
 &\leq \frac{1}{\eta T} (\mathbb{E}[L(\theta_1)] - \mathbb{E}[L(\theta_{T+1})]) + \frac{1}{T} \frac{Q}{2} \eta \sum_{t=1}^T \mathbb{E}[\|g_t\|^2] \\
 &\quad + \frac{1}{T} \sum_{t=1}^T \frac{Q}{2} \frac{\eta}{N^2 p^2} \tilde{\sigma}^2 \tilde{\sigma}_t^2 + \frac{1}{T} \mathbb{E} \left[\sum_{t=1}^T \|\nabla L(\theta_t)\| P_t(C_t)G \right],
 \end{aligned} \tag{50}$$

which finish the proof for the first claim.

By substituting $\tilde{\sigma} = p \frac{1}{\mu_{\text{tot}}} \sqrt{2 \sum_{t=1}^T \frac{C_t^2}{\tilde{\sigma}_t^2}}$ from Corollary 2, assume $\tilde{\sigma}_t = \Theta(1)$ and L is lower bounded, we can further

get

$$\begin{aligned}
 & \frac{1}{T} \mathbb{E} \left[\sum_{t=1}^T \|\nabla L(\theta_t)\|^2 \right] \\
 & \leq \frac{1}{\eta T} (\mathbb{E}[L(\theta_1)] - \mathbb{E}[L(\theta_{T+1})]) + \frac{1}{T} \frac{Q}{2} \eta \sum_{t=1}^T \mathbb{E}[\|g_t\|^2] \\
 & \quad + Q \frac{\eta}{N^2 \mu_{\text{tot}}^2} \frac{1}{T} \sum_{t=1}^T \tilde{\sigma}_t^2 \sum_{t=1}^T \frac{C_t^2}{\tilde{\sigma}_t^2} \\
 & \quad + \frac{1}{T} \mathbb{E} \left[\sum_{t=1}^T \|\nabla L(\theta_t)\| P_t(C_t) G \right] \\
 & = \mathcal{O} \left(\frac{1}{\eta T} \right) + \mathcal{O}(\eta) + \mathcal{O} \left(\frac{\eta T}{N^2 \mu_{\text{tot}}^2} \right) \\
 & \quad + \underbrace{\frac{1}{T} \mathbb{E} \left[\sum_{t=1}^T \|\nabla L(\theta_t)\| P_t(C_t) G \right]}_{\text{bias term}} \quad (51)
 \end{aligned}$$

and after setting $\eta T = N \mu_{\text{tot}}$ and $\eta = \frac{1}{N \mu_{\text{tot}}}$, we can reach the conclusion that the above bound is $\mathcal{O}(\frac{1}{N \mu_{\text{tot}}}) + \text{bias term}$ which finishes the whole proof.

A.7. On the optimal solution of minimizing Eq. (17)

The minimization problem is rewritten below ignoring the irrelevant constants

$$\min_{\tilde{\sigma}_1, \dots, \tilde{\sigma}_T} \sum_{t=1}^T \tilde{\sigma}_t^2 \sum_{t=1}^T \frac{C_t^2}{\tilde{\sigma}_t^2}. \quad (52)$$

The above problem can be transformed into an equivalent problem raised in Theorem 4.2 and Remark 4.1 of Wu et al. (2021) which we restate below

$$\min_{a_1, \dots, a_T} \sum_{t=1}^T \frac{a_t^2}{b_t^2} \sum_{t=1}^T \frac{1}{a_t^2} \quad (53)$$

And according to Remark 4.1 in Wu et al. (2021), an optimal solution to (53) is $a_t^2 = b_t$ which yields an optimal value of $(\sum_{t=1}^T \frac{1}{b_t})^2$. Going back to (52), we can define $a_t = \sigma_t / C_t$ and $b_t = 1 / C_t$ to transform (52) into (53). Thus, we know an optimal solution to (52) would be

$$a_t^2 = \frac{\tilde{\sigma}_t^2}{C_t^2} = b_t = \frac{1}{C_t}, \quad (54)$$

which gives

$$\tilde{\sigma}_t = \sqrt{C_t}. \quad (55)$$

A.8. Extension of Theorem 1 with local curvature assumption

In this section, we present a different version of Theorem 1 with a local curvature assumption

$$\begin{aligned}
 & \mathbb{E}_t[L(\theta_{t+1})] - L(\theta) \\
 & \leq \langle \nabla L(\theta_t), \mathbb{E}_t[\theta_{t+1} - \theta_t] \rangle + \frac{Q_t}{2} \mathbb{E}_t[\|\theta_{t+1} - \theta_t\|^2]. \quad (56)
 \end{aligned}$$

This assumption is not standard in optimization but the intuition is quite straightforward. The assumption can be understood as the neighborhood region around θ_t has a curvature bounded by Q_t , and the diameter of the neighborhood is vaguely defined by some statistics about $\theta_{t+1} - \theta_t$, which in turn depends on the algorithm choice. Overall, this is an optimistic assumption on both the algorithm and the problem. The motivation of such an assumption is to take account for the fact that the local curvatures of different iterates in neural network training are typically quite different.

With this assumption, we can rework Theorem 1 to obtain Theorem 2.

Theorem 2. Denote the objective function as $L(\theta) = \frac{1}{N} \sum_{i=1}^N f(\theta, x_i)$ and the clipped stochastic gradient at step t as $g_t = \frac{1}{p|X_t|} [\sum_{x \in X_t} \text{CL}(g_x; C_t)]$ where $g_x = \frac{\partial f(\theta_t, x)}{\partial \theta_t}$.

Assume (56) holds and each per-sample gradient is upper-bounded, i.e. $\|g_x\| \leq G, \forall t$. General dynamic DP-SGD (Algorithm 3) satisfies the following utility guarantee

$$\begin{aligned}
 & \mathbb{E} \left[\frac{1}{T} \sum_{t=1}^T \|\nabla L(\theta_t)\|^2 \right] \\
 & \leq \frac{1}{\eta T} \mathbb{E}[L(\theta_1)] - L(\theta_{T+1}) + \frac{\eta}{T} \sum_{t=1}^T \frac{Q_t}{2} \mathbb{E}[\|g_t\|^2] \\
 & \quad + \underbrace{\mathbb{E} \left[\frac{1}{T} \sum_{t=1}^T \|\nabla L(\theta_t)\| P_t(C_t) G \right]}_{\text{bias term}} + \underbrace{\frac{\eta}{p^2 N^2} \frac{1}{T} \sum_{t=1}^T \frac{Q_t}{2} \tilde{\sigma}_t^2 \tilde{\sigma}_t^2}_{D_2}. \quad (57)
 \end{aligned}$$

where $P_t(C_t)$ is the probability of a per-sample gradient being clipped with threshold C_t at θ_t , and the expectations are take over all randomness including gradient sampling and noise sampling.

Proof: The proof follows the same procedure as that of Theorem 1 with Q in (44) replaced by Q_t , i.e., we get the following version of (44)

$$\begin{aligned}
 \mathbb{E}_t[L(\theta_{t+1})] & \leq L(\theta_t) + \mathbb{E}_t[\langle \nabla L(\theta_t), (\theta_{t+1} - \theta_t) \rangle] \\
 & \quad + \mathbb{E}_t \left[\frac{Q_t}{2} \|\theta_{t+1} - \theta_t\|^2 \right] \\
 & \leq L(\theta_t) - \eta \langle \nabla L(\theta_t), \mathbb{E}_t[g_t] \rangle + \frac{Q_t}{2} \eta^2 \mathbb{E}_t[\|g_t\|^2] \\
 & \quad + \frac{Q_t}{2} \frac{\eta^2}{N^2 p^2} \tilde{\sigma}_t^2 \tilde{\sigma}_t^2. \quad (58)
 \end{aligned}$$

All the remaining steps are the same as those in Theorem 1 with Q replaced and thus we omit them.

Remark on the variance term D_2 : It is straightforward to see that just like in Theorem 1, we can minimize the corresponding variance term D_2 by substituting the $\tilde{\sigma}$ expression from Theorem 2 and tuning $\tilde{\sigma}_1, \dots, \tilde{\sigma}_T$. However, the minimization problem is slightly different due to Q_t , the problem is written below ignoring irrelevant constants

$$\min_{\tilde{\sigma}_1, \dots, \tilde{\sigma}_T} \sum_{t=1}^T Q_t \tilde{\sigma}_t^2 \sum_{t=1}^T \frac{C_t^2}{\tilde{\sigma}_t^2}. \quad (59)$$

This problem can also be transformed in to the form of 53 by defining $a_t = \sigma_t/C_t$ and $b_t = 1/(C_t\sqrt{Q_t})$. And according to the optimal solution $a_t^2 = b_t$, we have

$$a_t^2 = \frac{\sigma_t^2}{C_t^2} = b_t = \frac{1}{C_t\sqrt{Q_t}}, \quad (60)$$

which indicates

$$\tilde{\sigma}_t = \frac{\sqrt{C_t}}{Q_t^{1/4}}, \quad (61)$$

and thus

$$\mu_t = \frac{C_t}{\tilde{\sigma} \cdot \tilde{\sigma}_t} \propto \sqrt{C_t} Q_t^{1/4}. \quad (62)$$

Such a result indicates one should also change privacy budget of different steps according to local curvatures. And if assuming the local curvatures of different steps follow some general rules or distributions, one could design corresponding strategies to allocate the privacy budget. Yet, identifying such rules and distributions is a difficult task and could depend on the application domains. We hope the theoretical analysis here could help inspire future exploration in this direction.

A.9. Experimental Settings on Different Data Sets

MNIST (Lecun & Bottou, 1998) that contains 60000 training samples and 10,000 testing samples with ten balanced classes. Each gray-scale sample is stored as a 28×28 matrix. The classification model used in our experiments consists of two convolution layers and two fully connected layers. Following each convolution layer is a max-pooling layer with a pooling size of 2×2 . For activations, we use ReLU and for classification, we use softmax. Cross-entropy loss is used.

In the experiment, initial clipping value is set to 1.5 and learning rate is set to 0.15. We set $p = \frac{250}{60000}$ for the subsampling with independent Bernoulli trial. All the results are the average over 5 times repeated experiments.

FashionMNIST is a dataset of Zalando’s article images, serving as an alternative to MNIST dataset for benchmarking machine learning algorithms. It shares the same image size and structure of training and testing splits. As a result, we use the same experimental setup as MNIST. The only difference is that we specified a clipping value of 4 as the initial value.

IMDB For natural language processing or text analytics, the IMDB dataset contains 50K movie reviews. This is a binary sentiment classification dataset. We use a three-layer network with one embedding layer and two fully connected layers; this can be viewed as an MLP model because the embedding layer is a special implementation of fully connected layers. We train for 25 epochs with the DP-Adam optimizer, with the initial clipping value set to be 2.

NAME is a name classification dataset containing person names from 18 countries. It is available on Pytorch NLP tutorials⁴. We train a LSTM model to determine which country the given name belongs to. The name is treated as a sequence, and the characters are fed into LSTM one by one. We use a one-layer LSTM with hidden size 128 and embedding size 64 followed by a fully connected layer, an SGD optimizer with learning rate 2 and we train 50 epochs for each experiment, and the initial clipping value is set to be 1.5.

InfiniteMNIST and Federated Learning InfiniteMNIST is a dataset consisting of massive training samples derived from origin MNIST by applying different types of transformations. Such large scale dataset is suitable for a federated setting. We extract 250K and 500K images as two training data sets and simulate identical number of clients. Thus each client is not enough to train the model, but they can cooperatively learn a model via federated learning. We use the same network structure as in the experiment for MNIST for each client.

Federated Learning Algorithm Fed-SGD algorithm is used for optimization. For each round, we randomly sample clients with sampling rate $p = 1 \times 10^{-3}$ for the case of MNIST-250K and $p = 5 \times 10^{-4}$ for the case of MNIST-500K. Gradients are computed on each selected client and then sent to the server for aggregation. In this setting, local DP mechanism is required to protect client side gradients, and each client apply clipping and additive noise on local gradients before transmission. The server will aggregate noised gradients, which achieves central DP. The details is provided in the following Algorithm 5.

A.10. VGG network and Chest Radiographs

We evaluated VGG on chest radiographs classification task from the Paediatric Pneumonia dataset described in Ziller

⁴https://pytorch.org/tutorials/intermediate/char_rnn_classification_tutorial.html

Algorithm 5 Federated Dynamic DP-SGD Algorithm

Require: Clients set \mathcal{S} , DP budget (ϵ, δ) , client sampling rate p , dataset $X = (X_1, X_2 \dots X_{|\mathcal{S}|})$, training rounds T , hyper-parameters: ρ_μ, ρ_c and C_0 .

- 1: Compute μ_0 in Algorithm 1
- 2: **for** $t = 0, \dots, T - 1$ **do**
- 3: Compute $C_t = (\rho_c)^{-\frac{t}{T}} \cdot C_0$ according to (12)
- 4: Calibrate noise : $\sigma_t = \frac{C_0}{\mu_0} (\rho_\mu \cdot \rho_c)^{-\frac{t}{T}}$
- 5: Sample clients for the t -th iteration, i.e., $\mathcal{S}_t \in \mathcal{S}$ with Poisson sampling rate p .
- 6: **for** $k \in \mathcal{S}_t$ **do**
- 7: $g_{k,t} = \frac{1}{|\mathcal{S}_t|} (\sum_{x \in \mathcal{S}_t} (g_x; C_t) + \xi_{k,t})$ with $\xi_{k,t} \sim \mathcal{N}(0, \sigma^2 I)$
- 8: Send $g_{k,t}$ to the server.
- 9: **end for**
- 10: Server computes: $\theta_{t+1} = \theta_t - \eta \frac{1}{|\mathcal{S}_t|} (\sum_{k \in \mathcal{S}_t} g_k)$
- 11: **end for**

et al. (2021), which is a binary classification task, and the model attempts to predict whether the radiograph shows signs of pneumonia or not. For the classification task, following that in Ziller et al. (2021), we utilized the same model architecture in the private and nonprivate setting, namely a VGG-11 architecture. Following Ziller et al. (2021), batch normalization layers was disabled for both non-private and DP training.